Turbulent compressible axisymmetric flows computation with the K-Epsilon model

Bijan Mohammadi, J.H. Saiac

UNITÉ DE RECHERCHE
INRIA-ROCQUENCOURT

Rapports de Recherche

1992

25ème anniversaire

N° 1764

Programme 6
Calcul Scientifique, Modélisation et Logiciels numériques

TURBULENT COMPRESSIBLE AXISYMMETRIC FLOWS COMPUTATION WITH THE K-EPSILON MODEL

Bijan MOHAMMADI
Jacques-Hervé SAIAC

Octobre 1992

Institut National
de Recherche
en Informatique
et en Automatique

Domaine de Voluceau
Rocquencourt
B.P. 105
78153 Le Chesnay Cedex
France
Tél.:(1) 39 63 55 11

RR-1764

Turbulent Compressible Axisymmetric Flows Computation with the K-Epsilon Model

Calcul d'Ecoulements Axisymetriques Compressibles Turbulents avec le Modèle K-Epsilon

Bijan MOHAMMADI

INRIA-MENUSIN
Domaine de Voluceau B.P.105 - 78153 Le Chesnay (FRANCE)

Jacques Hervé SAIAC

INRIA-MENUSIN
Domaine de Voluceau B.P.105 - 78153 Le Chesnay (FRANCE)

Abstract

A new technique is proposed to compute axisymmetric flows. Turbulence modelling is done with a $k - \varepsilon$ model for high Reynolds number regions and a $k - L$ one-equation model for near-wall regions. Moreover, a new robust algorithm for the turbulent equations is presented. A hypersonic boundary layer on a cone and a detached fully turbulent base flow are presented as test cases.

Keywords: Axisymmetric Flows, Navier-Stokes Equations, Turbulence, Two-equation Model, Two-layer Approach.

Résumé

On propose une nouvelle technique pour le calcul d'écoulements axisymétriques. On utilise un modèle $k - \varepsilon$ pour la modélisation de la turbulence à grand nombre de Reynolds et un modèle $k - L$ à une équation pour les régions proches de corps solides. Les résultats numériques pour une couche limite hypersonique sur un cône et un écoulement détaché derrière une marche axisymétrique sont présentés.

Mots-Clés: Ecoulements Axisymetriques, Equations de Navier-Stokes, Turbulence, Modèle à deux Equations, Approche Bi-couche.

1 Introduction

In this paper we propose a new method for computing high speed turbulent axisymmetric flows. We consider the Reynolds averaged Navier-Stokes equations. These equations are closed by introducing a new viscosity for the fluid and by taking the Reynolds tensor parallel to the deformation one. Moreover, third order correlations are neglected and the velocity-temperature correlation is modeled by a gradient hypothesis[2]. To compute the eddy viscosity a two-equation $k-\varepsilon$ turbulence model is used. The $k-\varepsilon$ model used here is a generalization of the incompressible version of the model to the compressible case. It is well-known that the $k-\varepsilon$ model is not valid for regions near solid boundaries. The classical way to deal with this problem is to use some artificial boundary conditions called wall-laws rather than to compute the flow up to the wall. But, the classical wall laws technique fails when separation occurs. In this paper we use a two-layer approach[1]. The following techniques have been already successfully used to compute 2D flows[2,3]. Our aim is to extend our 2D model to the axisymmetric case in such a way to reduce to a minimum the additional modifications which have to be done on the existing 2D code. More precisely, the derivation of the axisymmetric NS solver is done by adding two simple routines to the 2D code.

In section II, we present the compressible Navier-Stokes equations in cylindrical coordinates, the $k-\varepsilon$ and the $k-L$ turbulence models. Section III is devoted to the description of the numerical methods. The Navier-Stokes solver is derived from an Euler solver by adding viscous perturbations. It is based on a finite element-finite volume approximation of the Navier-Stokes equations in conservation form. An upwind Osher-Riemann solver is used for the Euler part of the equations and second order accuracy in space is obtained limiting the gradients of the conservative variables by a MUSCL technique. The viscous parts of the equations are treated in a centered way. The solver is linearly implicit in time and the linear system is solved using a linear GMRES technique. Moreover, we use a block-diagonal preconditioning. The solver works on unstructured triangular grids.

For the turbulent equations, we propose a new robust algorithm which produces positive and bounded values for the turbulent quantities without using limiters. Indeed, the $k-\varepsilon$ system is unstable and if nothing is done to improve the stability of the discretized system, it may produce negative values. Our $k-\varepsilon$ algorithm is based on a splitting of the turbulent equations into transport and diffusion step and we treat the stability problem in the transport step. In section IV two hypersonic turbulent test cases of the Workshop on Hypersonic Flows for Reentry Problems are presented.

2 Governing Equations

We consider the Reynolds averaged axisymmetric Navier-Stokes equations in conservative form. Turbulence modelling is done by a two-equation $k-\varepsilon$ eddy-viscosity model[2].

2.1 Navier-Stokes Equations

Let $\rho, u_z, u_r, E, p, T, e$ be the density, the axial and radial components of the velocity, the total energy, the pressure and the temperature of the fluid. We consider the conservative form of the adimensionned Navier-Stokes equations governing newtonian compressible fluids. We suppose that the fluid motion is axisymmetric. That means that all of the θ-derivatives are zero. Moreover, the swirl or θ-component of the velocity is supposed to be zero. So, $W = (\rho, \rho u_z, \rho u_r, \rho E)$ being the vector of conservative variables, in cylindrical coordinates z, θ, r the Navier-Stokes equations in conservative forms are:

$$\frac{\partial}{\partial t}(W) + \nabla.F(W) = \nabla.N(W) + H(W) \tag{2.1}$$

with

$$W = \begin{pmatrix} \rho \\ \rho u_z \\ \rho u_r \\ \rho E \end{pmatrix},$$

$$F_z(W) = \begin{pmatrix} \rho u_z \\ \rho u_z^2 + p \\ \rho u_z u_r \\ (\rho E + p) u_z \end{pmatrix},$$

$$F_r(W) = \begin{pmatrix} \rho u_r \\ \rho u_r u_z \\ \rho u_r^2 + p \\ (\rho E + p) u_r \end{pmatrix},$$

$$N_z(w) = \begin{pmatrix} 0 \\ \tau_{zz} \\ \tau_{zr} \\ \kappa_{tot}\frac{\partial T}{\partial z} + u_z\tau_{zz} + u_r\tau_{zr} \end{pmatrix},$$

$$N_r(w) = \begin{pmatrix} 0 \\ \tau_{rz} \\ \tau_{rr} \\ \kappa_{tot}\frac{\partial T}{\partial r} + u_z\tau_{zr} + u_r\tau_{rr} \end{pmatrix},$$

and

$$H(w) = \begin{pmatrix} 0 \\ 0 \\ -\frac{\tau_{\theta\theta}}{r} \\ 0 \end{pmatrix}$$

with the following expressions for the tensor components:

$$\tau_{zz} = \mu_{tot}[2\frac{\partial u_z}{\partial z} - \frac{2}{3}(\nabla.u)],$$

$$\tau_{zr} = \mu_{tot}[\frac{\partial u_z}{\partial r} + \frac{\partial u_r}{\partial z}],$$

$$\tau_{rr} = \mu_{tot}[2\frac{\partial u_r}{\partial r} - \frac{2}{3}(\nabla.u)],$$

$$\tau_{\theta\theta} = \mu_{tot}[2\frac{u_r}{r} - \frac{2}{3}(\nabla.u)]$$

where

$$\nabla.u = \frac{\partial}{\partial z}u_z + \frac{1}{r}\frac{\partial}{\partial r}(ru_r),$$

$$p = (\gamma - 1)\rho E, E = T + \frac{1}{2}u^2,$$

$$\kappa_{tot} = \mu\frac{\gamma}{Pr} + \mu_t\frac{\gamma}{Pr_t},$$

$$\mu_{tot} = \mu + \mu_t,$$

$$\gamma = 1.4, Pr = 0.72, Pr_t = 0.9.$$

μ is the viscosity of the fluid given by the Sutherland law's, κ_{tot} is the total thermal conductivity, P_r and Pr_t are respectively the laminar and turbulent Prandtl numbers.

2.2 Turbulence Models

We propose, as for 2D plane flows, an extension of the two-layer model[1] to the compressible case. More precisely, a two-equation model is used for high Reynolds regions and a one-equation model for low Reynolds regions near the solid walls. We will present here briefly the turbulence model we use[2].

2.2.1 The High-Reynolds $k-\varepsilon$ Model

The $k-\varepsilon$ equations we consider read

$$\frac{\partial k}{\partial t} + u\nabla k - \frac{1}{\rho}\nabla(c_\mu \rho \frac{k^2}{\varepsilon}\nabla k) = S_k$$

$$\frac{\partial \varepsilon}{\partial t} + u\nabla \varepsilon - \frac{1}{\rho}\nabla(c_\varepsilon \rho \frac{k^2}{\varepsilon}\nabla \varepsilon) = S_\varepsilon$$

The above right hand sides contain the production and the destruction terms of k and ε.

$$S_k = c_\mu \frac{k^2}{\varepsilon} E - \varepsilon$$

$$S_\varepsilon = c_1 k E - c_2 \frac{\varepsilon^2}{k}$$

where the constants $c_\mu, c_1, c_2, c_\varepsilon$ are respectively equal to $0.09, 0.129, 1.92, 0.07$ and

$$E = \frac{1}{2}|\nabla u + \nabla u^t|^2.$$

The eddy viscosity is then given by

$$\mu_t = c_\mu \rho \frac{k^2}{\varepsilon} \tag{2.2}$$

2.2.2 The Low-Reynolds Model

The classical $k-\varepsilon$ model is valid under the hypothesis that the local Reynolds number is high. But it is not adequate to describe regions close to a solid wall where the local Reynolds number decreases. Moreover, classical wall laws techniques fail when separation occurs. On the other hand a two-equation low Reynolds $k-\varepsilon$ model will require too fine a mesh to describe the variations of the turbulent quantities in near-wall regions (especially ε). So we prefer an intermediate solution which consists to compute the flow near the solid wall by the following transport equation for the turbulent energy k

$$\frac{\partial k}{\partial t} + u\nabla k - \frac{1}{\rho}\nabla.(\mu_t \nabla k) = \mu_t E - D_{iss}$$

where

$$D_{iss} = \frac{k^{\frac{3}{2}}}{l_\varepsilon} \tag{2.3}$$

and

$$\mu_t = c_\mu \rho \sqrt{k} l_\mu. \tag{2.4}$$

l_μ and l_ϵ are two length scales containing the damping effects in the near wall regions.

$$l_\mu = \kappa c_\mu^{-3/4} y(1 - exp(\frac{-y^+}{c}))$$

$$l_\epsilon = \kappa c_\mu^{-3/4} y(1 - exp(-\frac{y^+}{2\kappa c_\mu^{-3/4}}))$$

where $c = 70$ and $\kappa = 0.45$.

3 Numerical Methods

We will first describe our 2D Navier-Stokes conservative solver. Then we explain how we take into account the axisymmetric corrections and finally we give a new algorithm to solve the $k - \varepsilon$ equations.

3.1 The Navier-Stokes Solver

The axisymmetric Navier-Stokes solver is an adaptation of a Finite volume-Galerkin 2D Navier-Stokes solver developed by P. Rostand and B. Stoufflet[10,11] for unstructured grids. For the convective part of the equations we use an upwind TVD. finite volume method based on an approximate Osher Riemann solver. The diffusive part is approximated in a centered way using a P_1 finite-element method. Because we are specially interested in steady flows, the time discretization scheme is linearly implicit and a local time step technique is used[10]. The linear system is preconditionned by the inverse of 4×4 block-diagonal part of the matrix and it is solved by a linear GMRES approach[9]. A summary description of the 2D solver is given in appendix.

3.2 Axisymmetric Corrections

The differences between the axisymmetric and the 2D integral form of the Navier-Stokes equations which we use come from the right hand side $H(W)$ which appear in 2.1 and from the infinitesimal area in the integrals ($rdrdz$ instead of $dxdy$). So, to adapt the solver to axisymmetric computations, we multiply the cell areas $|C_i|$, the triangle areas $|T_i|$ and the edge lengths $|E_i|$ by some radius r obtained from the radius of the nodes. We do that in the first part of the code where we compute the geometrical quantities.

We choose the following formula:

$|C_i|$ becomes $|C_i| * r_i$ where r_i is the second coordinate of the node s_i

$|T_i|$ becomes $|T_i| * \frac{r_1+r_2+r_3}{3}$

with r_1, r_2, r_3 the radius corresponding to the vertices of the triangle T_i

$|E_i|$ becomes $E_i * \frac{r_1+r_2}{2}$
where r_1 and r_2 are the radius of the extremities of E_i.
The other modifications which have to be introduce come from the additional source terms occuring in the equation 2.1. We introduce them explicitly (this means that we don't take it into account in the matrix). More precisely, for the momentum equation in u_z, we add to the right hand side:

$$-\int_{\partial c_i} \frac{2}{3}\mu_{tot} u_r n_z r d\gamma.$$

In the same way, to the right hand side of the momentum equation in u_r we add:

$$\int_{c_i} \frac{P}{r}.r dr dz - \int_{c_i} \frac{\tau_{\theta\theta}}{r} r.dr dz - \int_{\partial C_i} \frac{2}{3}\mu_{tot} u_r n_r d\gamma.$$

And finally, to the right hand side of the energy equation we add:

$$-\int_{\partial c_i} \frac{2}{3}\mu_{tot} u_z u_r n_z r d\gamma - \int_{\partial c_i} \frac{2}{3}\mu_{tot} u_r^2 n_r r d\gamma.$$

The above analysis enables us to reduce to a minimum the modifications on the existing 2D code.

3.3 Stabilization of the $k-\varepsilon$ Solver

Implementing the $k-\varepsilon$ model in a finite element framework involves several difficulties. The most important among these is, from the numerical point of view, the high instability of the discretized $k-\varepsilon$ equations. We know that the difficulties come from the resolution of the dynamical part (i.e. the convective operator and the source terms) of the equations and the viscous part is not really difficult to solve (by classical centered schemes). We have carefully studied[2,3,5] these dynamical parts and we have presented two new variables having very good numerical behaviour. More precisely, let

$$\varphi = \frac{\varepsilon^2}{k^3} \quad and \quad \theta = \frac{k}{\varepsilon}.$$

The dynamical equations for φ and θ come easily from those of k and ε. We denote $d/dt = \partial/\partial t + u\nabla$.

$$\frac{d\theta}{dt} = -aE\theta^2 + c$$

and

$$\frac{d\varphi}{dt} = -\alpha E\varphi\theta - \delta\frac{\varphi}{\theta} \leq 0$$

where $a = c_1 - c_\mu$, $c = c_2 - 1$, $\alpha = 3c_\mu - 2c_1$ and $\delta = 2c_2 - 3$ are positive constants and E is always positive. Therefore, θ stays bounded and positive[2] . Indeed, the θ

equation is a Riccati equation. So, for a positive initial condition $\theta_0 = k_0/\varepsilon_0$, it has an analytical solution:

$$\theta(t) = \frac{A(e^{-Bt}(\theta_0 - A) + \theta_0 + A)}{\theta_0 + A - e^{-Bt}(\theta_0 - A)} \tag{3.5}$$

where $A = \sqrt{c/a}$ and $B = \sqrt{acE}$.
The φ equation can also be integrated along the characteristic curves. Its solution, for a positive initial condition $\varphi_0 = \varepsilon_0^2/k_0^3$, is

$$\varphi = \varphi_0 exp((-\alpha E\theta - \frac{\delta}{\theta})t). \tag{3.6}$$

Therefore, φ stays positive and bounded too.
In the low Reynolds case ($y^+(= \sqrt{k}y\rho/\mu) \leq 200$), we can also find equations for θ and φ. But, the behaviour of φ and θ changes in the low Reynolds regions. This is in agreement with the fact that the $k - \varepsilon$ model is not valid in the near-wall region. So, the previous stability analysis can only be used for the fully turbulent regions. However, we can find another variable (also denoted by φ) such that:

$$\frac{d\varphi}{dt} = 0$$

in the low-Reynolds region. So, let,

$$\varphi = k^\alpha l_\mu^\beta$$

and suppose the kinematic viscosity $\nu = \mu/\rho$ is constant along the characteristic curves. Therefore, the φ equation is:

$$\frac{d\varphi}{dt} = k^{\alpha-1} l_\mu^{\beta-1} \{\alpha l_\mu \sqrt{k}(c_\mu l_\mu E - \frac{k}{l_\varepsilon})$$

$$-\beta \frac{\kappa y^2}{2\nu c} e^{-y^+/c}(c_\mu l_\mu E - \frac{k}{l_\varepsilon})\}.$$

So, if for instance we take

$$\alpha = \frac{y^+ e^{-y^+/c}}{2c(1 + e^{-y^+/c})} \quad \text{and} \quad \beta = 1 \tag{3.7}$$

where $y^+ = \sqrt{k}y/\nu$, then φ is stationary along the characteristics curves. The following picture shows a plot of α for $0 < y^+ < 200$. Numerical experiments were quite deceptive with this variable because α tends to zero near solid walls ($y^+ < 10$).

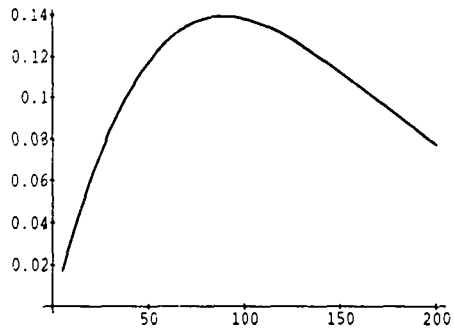

Figure 1: α vs. y^+

3.4 Turbulent Solver

To solve the k, ε equations, we make a splitting between the transport and diffusion part of the equations. We consider the source terms during the transport step using the stability analysis presented in the previous section. More precisely, we integrate the dynamical parts of the equations using the analytical solutions obtained for our new variables (θ and φ) in the previous section.

The diffusion parts of the equations are solved by a classical P^1 finite element technique. So, knowing ρ^n, u^n, k^n,ε^n, we propose the following algorithm to compute the turbulent quantities at the step $n+1$:

Algorithm (k, ε)

1. if $(y^+ > 200)$ *then*

a) Compute $\theta^n = k^n/\varepsilon^n$ *and* $\varphi^n = \varepsilon^{n2}/k^{n3}$

b) Compute $\theta^n(X^n)$ *and* $\varphi^n(X^n)$ *(i.e. convect* θ^n *and* φ^n, X^n *means at the beginning of the characteristic)*

c) Compute $\theta^{n+1/2}$ *and* $\varphi^{n+1/2}$ *by 3.5 and 3.6*

d) Compute

$$k^{n+1/2} = (\theta^{n+1/2})^{-2}(\varphi^{n+1/2})^{-1}$$

$$\varepsilon^{n+1/2} = (\theta^{n+1/2})^{-3}(\varphi^{n+1/2})^{-1}$$

endif

3. if $(y^+ \leq 200)$ *then*

Compute

$$k^{n+1/2} = \frac{k^n(X^n) + \Delta t \mu_t^n E^n}{1 + \Delta t \varepsilon^n / k^n}$$

4. Solve

$$\frac{k^{n+1}}{\Delta t} - \frac{1}{\rho^n}\nabla.((\mu + \mu_t^n)\nabla k^{n+1}) = \frac{k^{n+1/2}}{\Delta t}$$

$$\frac{\varepsilon^{n+1}}{\Delta t} - \frac{1}{\rho^n}\nabla.((\mu + c_\varepsilon \mu_t^n)\nabla \varepsilon^{n+1}) = \frac{\varepsilon^{n+1/2}}{\Delta t}$$

5. Solve

a) for $(y^+ \leq 200)$ *Compute* ε^{n+1} *by 2.3 and* μ_t^{n+1} *by 2.4*

b) for $(y^+ > 200)$ *Compute* μ_t^{n+1} *by 2.2*

In step 4, the degrees of freedom corresponding to nodes which are in low-Reynolds region are frozen for ε. The diffusive part of the equations are solved by a classical finite element method on P^1 triangles. Moreover, mass-lumping should be used. This treatment of the diffusion guarantees the positivity and boundedness of the solution, for Dirichlet boundary conditions, only if there is no obtuse angle in the mesh for all values of Δt and E.

4 Numerical Results

In the first case, we compute an hypersonic boundary layer on a cone. This case was the test case 1 of the Hermes Workshop at Antibes (France) in 1990 and 1991. The computation is compared to available data and occasionally to other computations. The second case consists of the base flow over an axisymmetric downward step behind the cone. In this case, the flow is fully detached, turbulent and hypersonic. The experiments were carried out at Imperial college (England) by P.A.Denman, J.K.Harvey and R.Hillier[6].

4.1 Flow over Slender Cone

The half angle of the cone is 7 degrees and its length is 0.578 m. The infinite mach number is 9.16 and the Reynolds number by meter is 5.510^7. The free stream temperature is 59.8 K and the wall temperature is fixed at 290 K. Experimental data are available for the pressure and the Stanton number (heat flux coefficient) at the wall. Also, computational local mach number and velocity profiles can be compared to the the experimental ones through the boundary layer.

Grid and Convergence

The mesh has 4865 nodes and 9433 triangles. The first point is at $5.10^{-6}m$ away from the wall. We have done two computations. A first one by taking into account the transition to turbulence and another computation where the flow is supposed fully turbulent (this means that the turbulence model was activated everywhere). In the first case, the transition from laminar to turbulent is arbitrarily assumed to occur between

$x = 0.1m$ and $x = 0.2m$ from the leading edge. This is done by multiplying the eddy viscosity by a function varying from zero to one through this zone. Experiment shows the transition occurs between $x = 0.6m$ and $x = 0.1m$. We found that changes around this position has little effects on the fully turbulent flow. The computation took about two hours on the CRAY II of the CCVR and 3000 iterations. The initial CFL number was 1 and it was increased to 100 during the iterations. Convergence was deemed to have occured when the global error based on the difference between the values of all of the variables in two successive iterations dropped by 5 orders of magnitude.

Surface Static Pressure

The time-averaged static pressure distribution, normalized by the free stream static pressure $p_\infty = 1/\gamma M_\infty^2$, computed on the cone surface is compared to the experimental recorded values in Fig. 3. Both computations give approximately the same result for the fully turbulent region. The pressure at the wall is then overestimated by about 10 percent. These results are in agreement with the results of the other contributors. In order to find the cause of this discrepancy, one of the contributors (Lawrence of NASA-Ames) studied several kind of sensitivity, but no explaination could be found[13]. He studied the following effects:

- Sensitivity to the variation of the inflow mach number gradient
- Sensitivity to grid spacing
- Sensitivity to wall temperature
- Sensitivity to turbulence model.

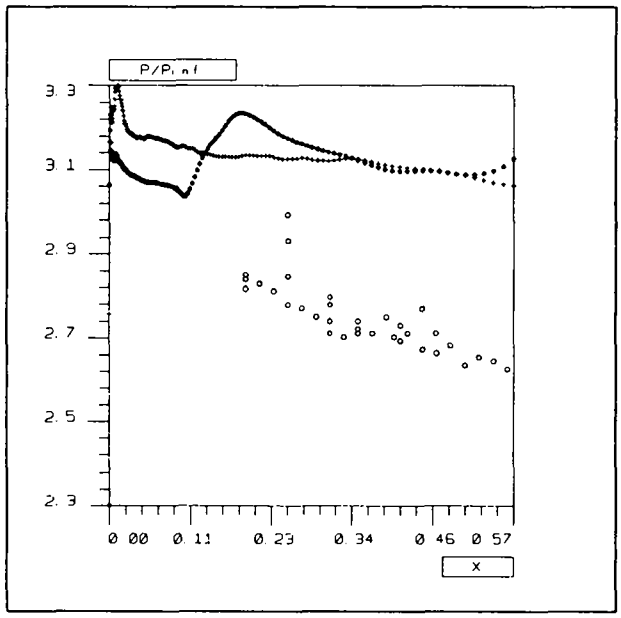

Figure 2: wall pressure(+ total, * trans, o data)

Heat Transfer Coefficient

The computed Stanton number ($St = \kappa \nabla T$) is compared to experimental data in Fig. 4. Because the transition is badly imposed, the maximum of the heat flux coefficient is displaced downstream. In the fully turbulent region, the heat flux is a little underestimated by both computations.

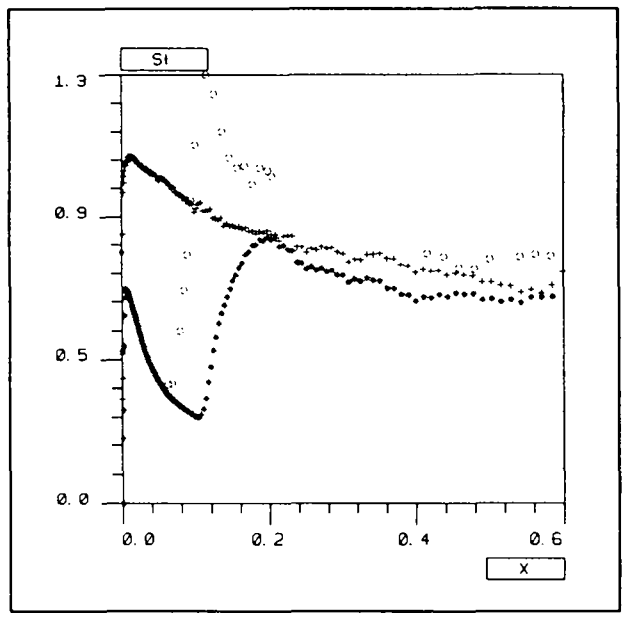

Figure 3: heat flux coef.(+ total, * trans, o data)

Cone Boundary Layer Profiles

Computed velocity profile (Fig. 5) and Mach number (Fig. 6) through the boundary layer are compared to experimental data at $x = 0.4m$ upstream of the base. The agreement is excellent in both cases.

For the base flow case, we begin the computation at $x = 0.18m$ upstream of the base and we take as inlet boundary condition the values obtained in the cone case.

4.2 Turbulent Base Flow

The previous cone is mounted on a shaft with diameter 0.04m smaller than the base of the cone. Therefore, the flow separates and a recirculation zone exists. The flow conditions at infinity and at the wall are the same than for the cone. Again, experimental data [6] for the pressure and the heat flux at the wall and the velocity and the Mach number profiles through the boundary layer are available.

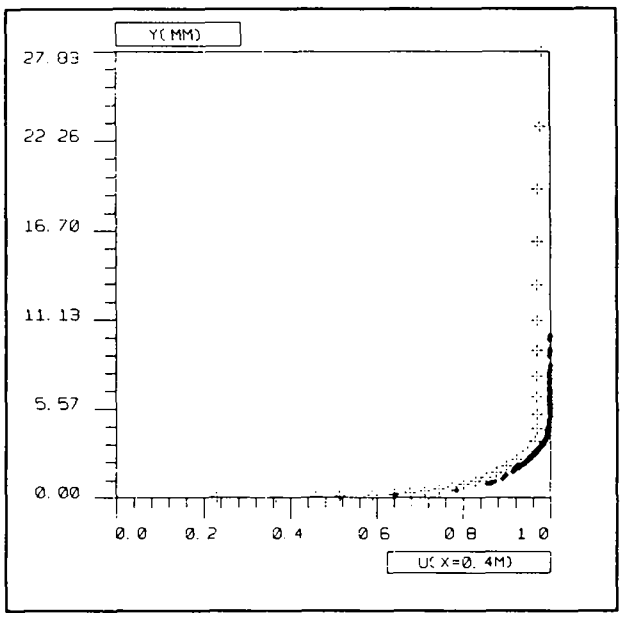

Figure 4: velocity profile (+ comp, * data)

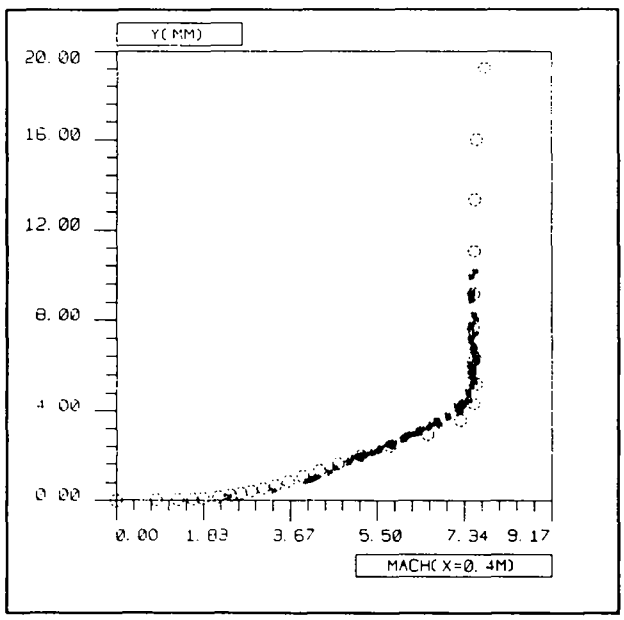

Figure 5: Mach number profile (o comp, * data)

We have also compared our results to the contribution of M.P.Netterfield[7]. His numerical method is based on a Spalding-Patankar's pressure correction to ensure mass continuity and a finite volume discretization of the equations. The equations are written in stationnary form and the nonlinear solver is line-implicit. He uses a $k-\varepsilon$ model for high-Reynolds regions and a law of the wall technique in near wall cells. Netterfield had some difficulties with the inlet boundary conditions because he did not compute the flow over the conical forebody. In particular, the experimental data did not give informations about turbulent quantities. Moreover, we expect the $k-\varepsilon$ model to give erronous results in the reattachment region because in such a region the Reynolds tensor is not parallel to the deformation one. So, considering the difficulty of the problem the comparison is not too much off the experimental results. The conclusion of the workshop was that this case is too difficult for the moment.

Grid and Convergence

The mesh has 9636 nodes and 18878 triangles. It was generated firstly by EMC2[8] automatical mesher of Hecht and Saltel which is based on a Voronoi algorithm. We have forced the mesh to be regular in near solid wall regions. We have locally refined this mesh (specially near solid wall) to improve the prediction of the heat flux coefficient at the wall. The first point is at about $1.e-4m$ away from the wall. As inlet boundary conditions, we use the results obtained in the cone case. The outlet boundary is placed at $x = 1.2m$. Neumann boundary condition is used at this boundary for all variables. At the top boundary free stream Dirichlet boundary condition is assumed. Globally, the computation took 6 hours on the CRAY II of the CCVR after 7000 iterations until the global error dropped by 4 orders of magnitude. Because the complexity of the flow, the convergence is quite hard to obtain. The initial CFL number was 1 and it was increased to 30 during the iterations.

Surface Static Pressure

The time-averaged static pressure distribution, normalized by the free stream static pressure $p_\infty = 1/\gamma M_\infty^2$, computed in the base region is compared to the experimentally recorded values and to the results of M.P.Netterfield[7] in Fig. 8. In the plot, $x = 0$ refers to the cone/sting corner. The flow reattachment is about $0.043m$ far from the corner.

Heat Transfer Coefficient

The computed Stanton number is compared to experimental data in Fig. 9. As it was expected the recirculation length is underestimated. However, we find the correct level of the heat flux coefficient after reattachment. The agreement is better for the two-layer approach. Another difficulty comes from the fact that in reattachment region the flow seems to be unsteady[6].

Pitot Pressure Profiles

Computed pitot pressure profiles, normalized by the free stream static pressure, through the boundary layer at $50mm$ and $100mm$ from the cone/sting corner are compared to

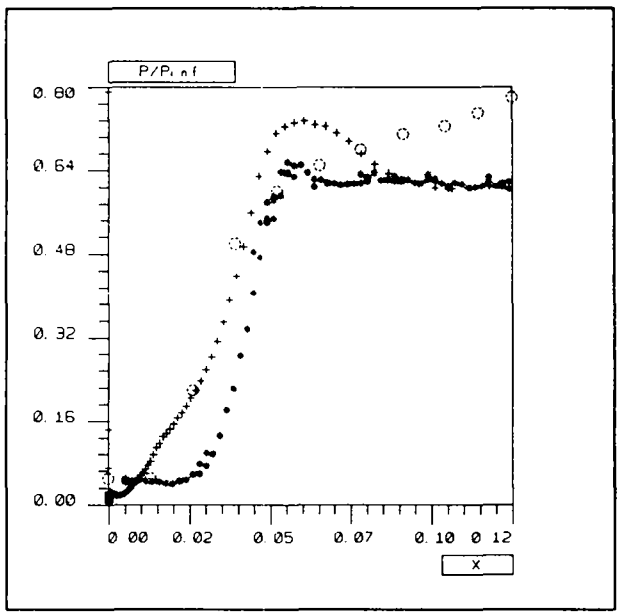

Figure 6: wall pressure (+ comp., * Hillier, o Netterfield)

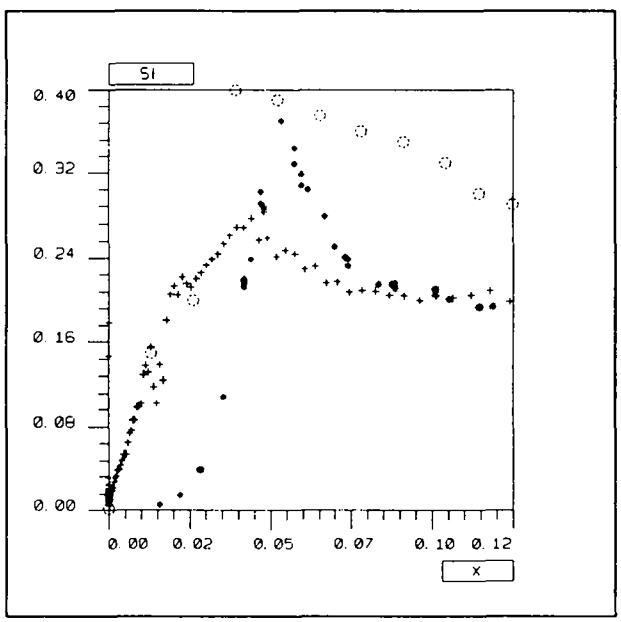

Figure 7: heat flux coef.(+ comp, * Hillier, o Netterfield)

experimental data in Fig. 10 and Fig. 11. The pitot pressure is computed from the local Mach number and static pressure by means of Rayleigh pitot formula:

$$\frac{p_t}{p_w} = (\frac{(\gamma+1)M^2}{2})^{\gamma/(\gamma-1)}(\frac{\gamma+1}{2\gamma M^2-(\gamma-1)})^{1/(\gamma-1)}$$

where $\gamma = 1.4$. p_w is the surface static pressure.

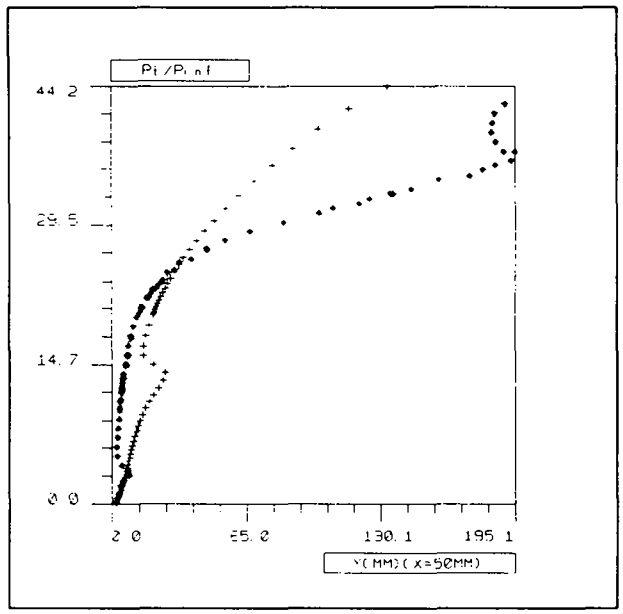

Figure 8: normalized pitot pressure at 50.mm (+ comp, * Hillier)

5 Conclusions

A new technique for computing axisymmetric flows and a new robust algorithm for the $k-\varepsilon$ equations have been presented. In near-wall regions, ε is computed using an algebraic expression rather than by solving a low-Reynolds ε equation. The solver is applied to two hypersonic test cases from the Workshop on Hypersonic Flows for Reentry Problems and satisfactory results are obtained. In particular, no stability or positivity problems have been encountered.

6 Appendix: 2D NS Solver

We give now a summary description of the 2D Navier-Stokes solver [10,11,12]. We consider the conservative NS equations 2.1 with $H(W) = 0$. Let $\Omega_h = \cup_j T_j$ a discretization by

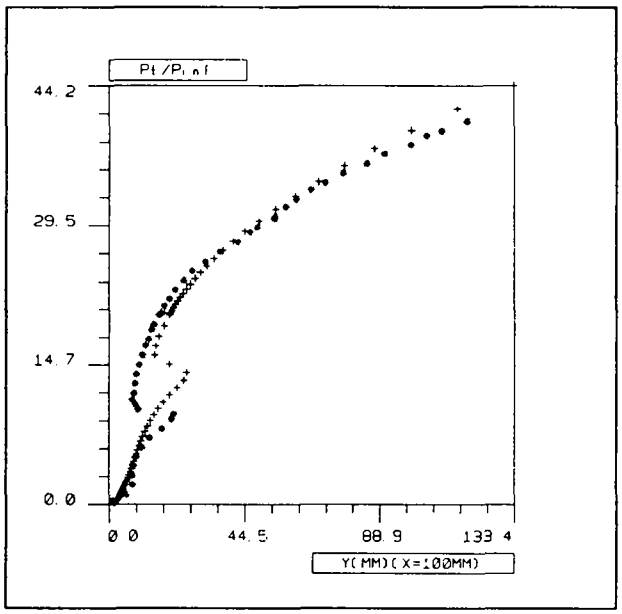

Figure 9: pitot pressure at 100.mm (+ comp, * Hillier)

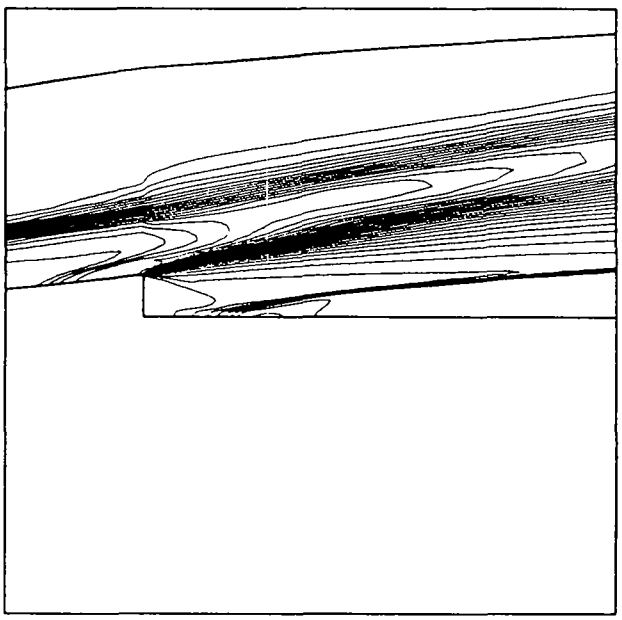

Figure 10: p/p_∞ contours

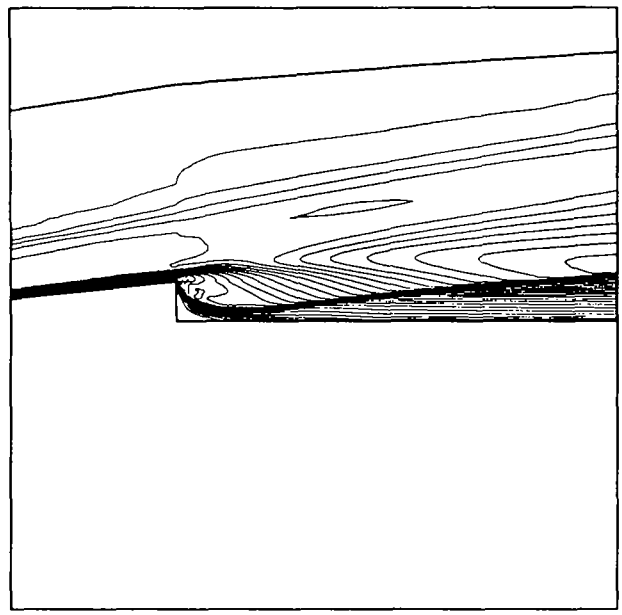

Figure 11: Mach number contours

triangles of the computational domain Ω and let $\Omega_h = \cup_i C_i$ its partition in cells, built for a node s_i by taking the medians not originating from s_i of the triangle surrounding it. Thus, we could associate to each $w_h \in V_h$, where V_h is the set of the continuous P^1 functions on our triangulation, a w'_h piecewise constant function on cells by

$$w'_h|C_i = \frac{1}{|C_i|}\int_{C_i} w_h.$$

Conversely, knowing w'_h piecewise constant, w_h is obtained as $w_h(S_i) = w'_h|C_i$. If we suppose that F varies linearly on each triangle, the classical weak formulation of NS involving V_h : Find $W_h \in (V_h)^4$ such that $\forall \phi_h \in V_h$

$$\int_\Omega \frac{\partial W_h}{\partial t}\phi_h - \int_\Omega (F_h - N_h)(W_h)\nabla(\phi_h)$$

$$+ \int_{\partial\Omega}(F_h - N_h)\cdot n\phi_h = 0 \qquad (6.8)$$

is equivalent to its Petrov-Galerkin weak formulation obtained by taking in the convective part of 6.8 for ϕ_h the characteristic function of C_i. Hence, after an explicit time integration we have for all nodes s_i :

$$|C_i|(\frac{W^{n+1} - W_i^n}{\Delta t}) + \int_{\partial C_i} F_d(W^n)\cdot n = R.H.S.$$

For

$$R.H.S. = -\int_{\Omega_h} N(W^n)\nabla(\phi_h) + \int_{\partial\Omega} N(W^n)\cdot n\phi_h$$

we use a centered scheme. Moreover, $F_d(W_h^n) = F(W_{\partial\Omega}$ on $\partial C_i \cap \partial\Omega$ and elsewhere F_d is a piecewise constant approximation of $F(W)$ verifying

$$\int_{\partial C_i} F_d \cdot n = \sum_{j\neq i} \Phi(W'|_{C_i}, W'|_{C_j}) \int_{\partial C_i \cap C_j} n.$$

Writing B the jacobian of F, we take for Φ the Osher proposition

$$\Phi_{Osher}(u,v) = \frac{1}{2}(F(u) + F(v) - \int_v^u |B(w)|dw)$$

where the integral is evaluated along a path piecewise parallel to characteristics. Spatial second order accuracy is obtained by the use of a MUSCL like extension using upwinded gradients. Such an explicit scheme gives slow convergence to a steady state because

we are limited by a CFL of order 1. In order to avoid this restrictive condition, we use a linearly implicit scheme

$$M(W^n)\delta W^{n+1} = b \tag{6.9}$$

where

$$\delta W^{n+1} = W^{n+1} - W^n,$$

$$b = \int_\Omega N_h \nabla\phi_h - \int_{\partial\Omega}(F_d - N_h)(W^n)\cdot n$$

and

$$M = \frac{\Delta t}{|C|} I + \frac{\partial(F_d - N)}{\partial W}(W^n).$$

The boundary conditions are taken into account in the matrix and in the right hand side of 6.9.

7 References

1. Patel V.C., Chen H.C., *Near-wall turbulence models for complex flows including separation*, AIAA Journal vol. 29, no. 6, June 1988.

2. Mohammadi B., *A stable algorithm for the $k-\varepsilon$ model for compressible flows*, 1990, INRIA report num. 1355.

3. Mohammadi B., *Complex turbulent flows computation with a two-layer approach* , 1991, to appear in Int. J. Num. Meth. Fluids.

5. Cardot B., Mohammadi B., Pironneau O., *A Few tools for the implementation of turbulence models in Navier-Stokes solvers.* Incompressible CFD-Trends and Advances, eds Max D. Gunzburger and R.A.Nicolaides Cambridge University Press 1991.

6. Denman P.A., Harvey J.K. and Hillier R., *Hypersonic Boundary Layer and Base Flow, Workshop Test Problems 1 and 2*, Proc. of the Workshop on Hypersonic Flows for Reentry Problems, january 22-26, 1990, Antibes (France), Vieweg Ed. to appear.

7. Netterfield M.P., *Computation of Hypersonic Turbulent Flow over Rearward facing Step*, Proc. of the Workshop on Hypersonic Flows for Reentry Problems, january 22-26, 1990, Antibes (France), Vieweg Ed. to appear.

8. Saltel E., Hecht F.,*EMC2, un Logiciel d'Edition de Maillages et de Contours Bidimensionnels*, INRIA technical report num. 118, 1990.

9. Saad Y. and Schultz M., *GMRES: A Generalized Minimum Residual Algorithm for Solving Nonsymmetric Linear Systems*, SIAM Journal of Scientific and Statistical Computing, Vol. 7, No. 3, 1986, pp. 856-869.

10. Rostand Ph.,*Sur une Méthode de Volumes Finis en Maillage Non Structuré pour le Calcul d'Ecoulements Visqueux Compressibles*, PhD Thesis, University of Paris VI, 1989.

11. Stoufflet B., Rostand P.,*TVD schemes to compute compressible viscous flows on ustructured meshes* , Notes on Numerical Fluid Mechanics, Vol. 24, pp. 510-520, Vieweg, Braunschweig, 1989.

12. Pironneau O.,*Finite Element Methods for Fluids*, Masson Ed., 1989.

13. Lawrence S. L., *Hypersonic Cone Flow Prediction Using an Implicit Upwind Space-Marching Code*, Proc. of the Workshop on Hypersonic Flows for Reentry Problems, january 22-26, 1990, Antibes (France), Vieweg Ed. to appear.

ISSN 0249-6399